The 35th Computational Fluid Dynamics Symposium
Your Paper No. C02-5

A Weak-Coupling CIP/IB Method for Free-Surface Flow Interacting with Flexible Structures

◯ Zhang, Jiantao,
School of Environment and Society,
Tokyo Institute of Technology,
4259 Nagatsutacho, Midori Ward, Yokohama, Kanagawa 226-0026,
zhang.j.am@m.titech.ac.jp

Nakamura, Takashi,
School of Environment and Society,
Tokyo Institute of Technology,
4259 Nagatsutacho, Midori Ward, Yokohama, Kanagawa 226-0026,
tnakamur@depe.titech.ac.jp

In this paper, we propose a numerical model to computer free-surface flow interacting with flexible structures. The model combines a constrained interpolation profile method to capture the multiphase interface with an immersed boundary method, which accurately enforces the no-slip and no-penetration boundary condition. The Navier-Stokes equations and nonlinear Euler-Bernoulli structural equations, where inextensibility condition is strictly preserved, are both discretized by FDM and coupled in a weak way. The performance of this method is validated through several numerical experiments. We simulate the flow past circle cylinder, study the dam break flow, and investigate the hanging pendulum in vacuum. In all validation cases, the numerical results of each module are compared, separately and respectively, with previous experimental results and numerical results, and good agreements are achieved, which show good ability of free surface capturing, hydrodynamic force calculation, and structure modelling. With the weak coupling, the flexible filament flapping in a uniform fluid flow is simulated, where the motion of the deformable structures and vortex in fluid field is checked. Finally, we apply the method to a hydroelastic water entry with a flexible plate impacting on static free water surface.

1. Introduction

The fluid-structure interaction (FSI) between free-surface flow and flexible structures is ubiquitous in nature and engineering, in which the interface between liquid and gas coupling with motion and deformation of flexible structures. Examples are aquatic vegetation canopy flows in river[1], sea-ice rheology[2], aircraft ditching and capillary origami[3]. Precisely computations of the liquid-gas interface and displacement and velocity of structure are vital to reveal the physical mechanism behind these phenomena.

In order to deal with multiphase fluid interface, e.g. liquid-gas interface, several strategies have been proposed, which can be divided into two main categories, namely, interface tracking method and interface capturing method. Marker-and-cell (MAC) method[4] and front tracking method[5,6] are two widely used interface tracking methods, where particles or Lagrangian points are evenly distributed to represent the liquid-gas interface at initial moment. However, when the surface deformation is large, the distribution of representing particles or points become either too tight or too loose, which causes inaccuracy. Meanwhile, several techniques use marker function to represent interface implicitly, known as level set (LS) method[7,8], volume of fluid (VOF) method[9,10], phase field (PF) method[11,12], and constrained interpolation profile (CIP) method[13,14,15]. In LS method, a reinitialization process is required to keep the LS function the shape of signed distance function. The original VOF method advances the marker function in a Lagrangian way, thus achieving a good mass conservation and relatively sharp interface, while the interface needs to be reconstructed by methods, such as SLIC and PLIC. In PF method, the mathematically sharp interface is simulated by a diffuse interface with finite thickness which related to mesh size. Meanwhile, CIP is another simple way to solve the marker function which not only calculates the advection of marker but also that of its spatial derivatives. Together with a shifting method with local characteristic flow velocity, CIP method can achieve results with less oscillation and diffusivity.

Recently, immersed boundary (IB) method, which uses non-conformal mesh, is widely utilized to simulate the FSI. The original IB method is proposed by Peskin[16,17] to discover the blood flow in heart valve. Unlike the conformal mesh methods, where meshes are aligned with the fluid-solid interface, IB method uses Eulerian mesh for fluid domain, while using freely moving Lagrangian points for structures. Therefore, IB method avoids the time-consuming mesh regeneration and mesh unevenly redistribution during largely structural deformation, which brings computational inaccuracy and instability. The essential idea of IBM is adding a volumetric force in the momentum equation, which represents the existence of solid structure among fluid. The variables along interface are transferred from fluid to solid through a smoothed Dirac function, and vice versa. A penalty version of IB method has been proposed and used in several applications of structure with mass[18,19]. Meanwhile, penalty IB method uses two large penalty parameter, which is a stiff system, requiring restricted small time step. To avoid this, Mohd-

Copyright © 2021 by JSFM

Yosuf[20] developed a method that directly extracts the force to satisfy the kinematic boundary condition on fluid-structure interface, known as direct force method. In most direct forcing method, the volumetric force in momentum equation is computed explicitly where the penetration of streamlines into solid surface occurs due to the no-slip boundary condition on fluid-solid interface enforced with errors. Ren[21] proposed an implicit direct forcing method which enforces the no-slip boundary condition accurately.

Though several researches adequately investigated the flexible structures interacting with the single phase flow[22,23], there are relatively few research conducted on interaction of flexible structures with multiphase flow due to the physical complexities and computational difficulties. Under such configuration, hydrodynamic force are exerted on flexible structures by different fluid phases with large fluid density ratio, such as water and air up to 1000. On the other hand, at which the three phases, liquid, gas, and solid meet, a moving contact line on structure surface exists, at which the elastocapillarity plays an important role[24]. A class of Lagrangian-Lagrangian configurations are developed to simulate such process, where fluid phase and solid phase are all represented, using meshless particle method, such as smoothed particle hydrodynamics (SPH)[25,26,27] and moving particle semi-implicit (MPS)[28,29]. Eulerian-Lagrangian methods using uniform Cartesian meshes have drawn attentions recently. In 2013, Liao & Hu[30] combined an explicit direct forcing IB method with a finite element method (FEM) based structure solver and used a improved tangent of hyperbola for interface capturing (THINC) method[31] for capturing free surface to simulate the slothing tank with elastic rod. However, in order to calculate the hydrodynamic force accurately, they needed to couple an extra virtual structure model, which places finer virtual particles around real structure. Yang et al.[32] simulated the dam break with elastic obstacle using a LS method and a immersed structural potential method (ISPM). Very recently, He et al.[33] proposed a pressure correction method for a velocity reconstruction IB method, preventing the fluid leakage during simulation of water impinging onto a plate.

In this paper, we develop a numerical model, which consists of a CIP method and an implicit direct forcing IB method, for the simulation of interaction between multiphase interface with flexible structure, as seen in Figure 1. The CIP model is used to advect the marker function which distinguish the gas phase from liquid phase by an immiscible interface. The use of the implicit direct forcing IB method can strictly enforce the no-slip and no-penetration boundary condition on the fluid-solid interface and thus avoid the streamline penetration of fluid into solid. The last, a nonlinear structure equation is solved to modify the position and velocity of flexible structure under the force from fluid phases as dynamic boundary condition and offers the kinematic boundary condition to fluid phases. A variety of numerical experiments, including flow past circle cylinder, dam break flow, hanging filament in vacuum, flow past flexible filament and hydroelastic water entry, are simulated.

The organization of the paper is as follows: We present the governing equations in Section 2., including those of interface evolution, fluid dynamics and structural dynamics. Then, we give a brief introduction of the numerical models in Section 3. We present our results of validation in Section 4. numerical simulation in Section 5.. The final section 6. includes the summary and conclusion of this study and suggested future works.

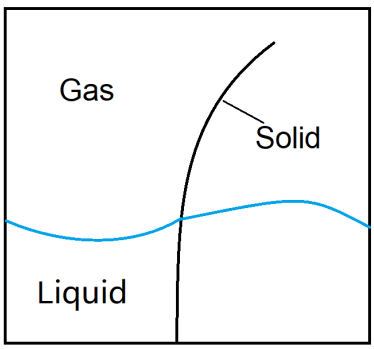


Fig. 1: Schematic diagram of the interaction between free surface and flexible structure.

2. Governing equations

2.1 Interface capturing equations

We investigate here free-surface flow with gas and liquid, e.g. air and water, both considered incompressible. The evolution of interface with time is modeled by the advection equation of volume fraction C, as,

$$\frac{\partial C}{\partial t} + \mathbf{u} \cdot \nabla C = 0 \tag{1}$$

where $\mathbf{u}$ is flow velocity. In practice, the volume fraction is of liquid, C_L. The volume fraction for gas, C_G, is consequently computed by $C_G = 1 - C_L$.

2.2 Navier-Stokes equations

The motion of fluids are governed by the dimensionless continuity equation and Navier-Stokes equations,

$$\nabla \cdot \mathbf{u} = 0, \tag{2}$$

$$\rho(\frac{\partial \mathbf{u}}{\partial t} + \mathbf{u} \cdot \nabla \mathbf{u}) = -\nabla p + \frac{1}{Re}\nabla \cdot [\mu(\nabla \mathbf{u} + \nabla \mathbf{u}^T)] - \frac{\rho}{Fr}\mathbf{j} + \mathbf{f}_{ib}$$

where $\mathbf{j}$ represents the vertical direction. $\mathbf{f}_{ib}$ represents the volumetric correction force in momentum equations from IB method, to account for the existence of flexible structure immersed in the liquid and gas. The dimensionless averaged density ρ and viscosity μ are defined as,

$$\rho = C_L + \lambda_{\rho,G} C_G \tag{3}$$

$$\mu = C_L + \lambda_{\mu,G} C_G \tag{4}$$

where $\lambda_{\rho,G} = \rho_G/\rho_L$ and $\lambda_{\mu,G} = \mu_G/\mu_L$ are the density and viscosity ratio of the gas to the liquid, respectively.

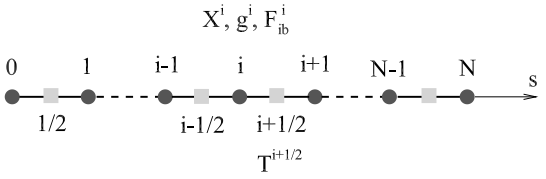


Fig. 2: Schematic diagram of a flexible filament in Lagrangian coordinate system.

Copyright © 2021 by JSFM

The fluid properties of the liquid are used to define the dimensionless number groups: Reynolds number $Re = \rho_L UL/\mu_L$, $Fr = U^2/gL$, where g is gravitation acceleration

2.3 Structure equations

The motion and deformation flexible structure are modeled the following dimensionless structure equation, written in a Lagrangian form, as seen in Figure 2. The structure in our study are inextensible, thus an inextensibility condition is constrained during the computation as follows,

$$M_\rho \frac{\partial^2 \mathbf{X}}{\partial t^2} = \frac{\partial}{\partial s}(T\frac{\partial \mathbf{X}}{\partial s}) - \frac{\partial^2}{\partial s^2}(K_b \frac{\partial^2 \mathbf{X}}{\partial s^2}) + \frac{1}{Fr}\mathbf{g} - \mathbf{F}_{ib} \quad (5)$$

$$\frac{\partial \mathbf{X}}{\partial s} \cdot \frac{\partial \mathbf{X}}{\partial s} = 1 \quad (6)$$

where s is the Lagrangian coordinate of arclength, $\mathbf{X} = (X(s,t), Y(s,t))$ is the position of Lagrangian point of structure in Eulerian coordinate, T is the dimensionless tensile force, K_b is the dimensionless bending rigidity, F_{ib} is the dimensionless IB method force exerted on the Lagrangian points by the surrounding fluid, M_ρ is the ratio of the linear density difference between solid and fluid to that of fluid, i.e. $(\rho_s - \rho L)/\rho L$.

3. Numerical modeling

3.1 Coupling boundary condition

In the simulation of fluid-structure interaction, the kinematic and dynamic boundary condition are obeyed on the interface which separating fluid and solid part.

The kinematic boundary condition is,

$$\mathbf{u}_\Gamma^f = \mathbf{u}_\Gamma^s, \quad (7)$$

where $\mathbf{u}$ represent velocity, f represents fluid phase, s represents solid phase, and Γ represents the fluid-solid interface. This boundary condition presents no slip and no penetration on fluid-solid interface.

The dynamic boundary condition is

$$\boldsymbol{\sigma}_\Gamma^f = \boldsymbol{\sigma}_\Gamma^s, \quad (8)$$

where $\boldsymbol{\sigma}$ represents stress on fluid-solid interface.

3.2 Immersed boundary method

In order to couple the fluid flow and structural motion and deformation, we use immersed boundary (IB) method which easily allows one to handle complex geometry on a non-comformal mesh, by introducing an body force $\mathbf{f}_{ib}$ in momentum equation. This force approximates the force that the flexible structure exert on the surrounding flow. The variables, velocity and force, on the interface are exchanged by using Dirac delta function, which can be written as,

$$\mathbf{U}_{ib}(s,t) = \int_\Omega \mathbf{u}(\mathbf{x},t)\delta(\mathbf{x} - \mathbf{X}_{ib}(s,t))d\mathbf{x}, \quad (9)$$

and

$$\mathbf{f}(\mathbf{x},t) = \int_\Gamma \mathbf{F}_{ib}(s,t)\delta(\mathbf{x} - \mathbf{X}_{ib}(s,t))ds, \quad (10)$$

where Ω is fluid domain, Γ is fluid-structure interface, and $\mathbf{U}_{ib}(s,t)$ and $\mathbf{F}_{ib}(s,t)$ are velocity and force on Lagrangian points.

In practice, a discretized Dirac delta function replaces the Dirac delta function, as,

$$\delta(r) = \begin{cases} \frac{1}{8}(3 - 2|r| + \sqrt{1 + 4|r| - 4r^2}) & |r| \le 1, \\ \frac{1}{8}(5 - 2|r| + \sqrt{-7 + 12|r| - 4r^2}) & 1 < |r| \le 2, \\ 0 & |r| > 2. \end{cases} \quad (11)$$

Here, we use the IB method proposed in[21], which allows us to keep an accurate no-slip boundary condition on fluid-structure interface without streamline penetration. In multiphase flow, where the density ratio of fluids is large, for example, water and air, the acceleration of gas is much larger than liquid, which will cause instability in computation. Therefore, we directly calculate the extra acceleration instead of body force in momentum equation. The corrected fluid velocity, equaling the velocity of corresponding structure point, is computed as follows[34],

$$\mathbf{u}^f = \mathbf{u}^* + \Delta t \rho \mathbf{a}^f. \quad (12)$$

4. Validation

We investigate the convergence and accuracy properties of the method, and validate each functions and coupling by simulating benchmark cases as, flow past circle cylinder, dam break, and hanging pendulum in vacuum.

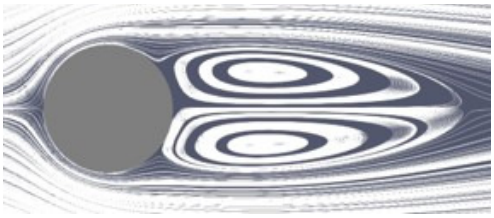


Fig. 3: Streamline of flow past static circle cylinder at $Re = 40$.

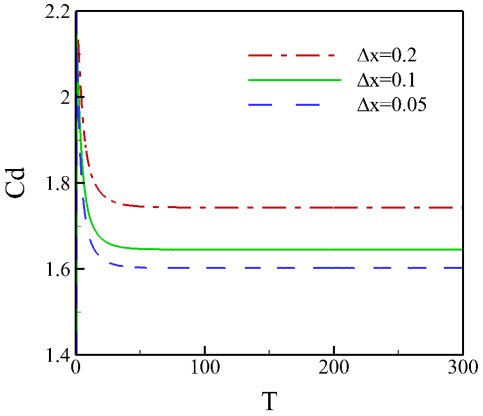


Fig. 4: Evolution of drag force coefficient with time under three different mesh sizes $\Delta x = 0.2D$ (dash-dotted), $0.1D$ (solid), and $0.05D$ (dash).

Copyright © 2021 by JSFM

Literature	C_d	L_r
Lima et al.[35]	1.54	2.55
Xu & Wang[36]	1.66	2.21
Wang et al.[37]	1.66	2.35
Ren et al.[21]	1.59	2.33
Liu et al.[38]	1.64	2.30
Present($\Delta x = 0.2D$)	1.74	2.68
Present($\Delta x = 0.1D$)	1.64	2.31
Present($\Delta x = 0.05D$)	1.60	2.29

Tab. 1: Comparison of drag force coefficient C_d and eddy length L_e at $Re = 40$.

4.1 Flow past circle cylinder

The convergence and the accuracy of force calculation of the method are tested by simulating static circle cylinder of diameter D in the incoming flow with velocity U. We choose D and U as the characteristic length and velocity. The computational domain is 60×30, and is resolved by uniform mesh with three different mesh size $\Delta x = 0.2D$, $0.1D$, and $0.05D$. The left boundary is inflow boundary condition with constant velocity U. The right boundary is convective boundary condition. Both upper and lower boundaries are no-penetration boundary condition. The time step is set at 0.002.

We simulate the flows at $Re = 40$, which with Reynolds number under critical value for periodic vortex shedding. A pair of eddies is attaching to the downstream area of the cylinder with constant length when the flow comes to steady. The results are compared with literature quantitatively in terms of drag force coefficient, C_d, and the length of eddy, L_e. The drag force coefficient is defined as,

$$C_d = \frac{F_d}{\frac{1}{2}\rho U^2 D}, \tag{13}$$

where F_d is the net force exerted on circle cylinder along the streamwise direction. Figure. 3 shows the flow pattern at dimensionless time $T = 100$, when the flow is steady. Figure. 4 shows the time evolution of drag force coefficient with three sets of mesh sizes, which presents convergent results. Table 1. present our numerical results under mesh size $\Delta x = 0.2D$, $0.1D$, and $0.05D$ with previous studies[35,36,37,21,38]. The comparison shows our results achieve good agreement with literature, suggesting the accuracy of force calculation of our method.

4.2 Dam break

We examine the capacity of our method in capturing the moving immiscible multiphase interface by simulating the two dimensional dam break, which has been extensively investigated both in computation[39] and experiment[40]. A water bulk collapses and flows under the effect of gravitation, as seen in Figure. 5. The height and width of water bulk is set to be same as L and used as the characteristic length. The computation domain is 10.5×1.75. The gravity acceleration g is used as characteristic acceleration. Thus, Froude number $Fr = U^2/gL$ is identical. The physical properties of liquid and gas phase is the same as water and air respectively. Those of water are taken as characteristic



Fig. 5: Snapshots of collapsed water bulk at different dimensionless time, T = (a) 0.0, (b) 1.7, (c) 3.3, and (d) 5.1.

quantities, which makes Reynolds number $Re = \rho UL/\mu$ equaling 37616 in calculation. However, the surface tension force between water and air is ignored here, since the Weber number, We, is large in this case. The mesh size and time step are 0.00875 and 0.0001. The snapshots of the results are shown in Figure. 5.

Figure. 6 shows the evolution of the wave front of the collapsed water bulk along x-direction with dimensionless time. As can been, our results compare well with previous numerical[39] and experimental results[40], although the wave front runs slightly faster than others. The ignorance of surface tension effect is a potential reason to this.

4.3 Hanging pendulum in vacuum

We perform the hanging pendulum under the effect of gravitation in vacuum, as in Fig. 7, to examine the accuracy of our method in modelling geometrical nonlinear structure. With a initial position away from the equilibrium, the hanging pendulum will swing under a gravitation force. Since there is no ambient fluid, and consequently energy loss, the swinging will continue in a periodic way.

In the simulation, 101 Lagrangian points are used to resolved the pendulum uniformly with the bending

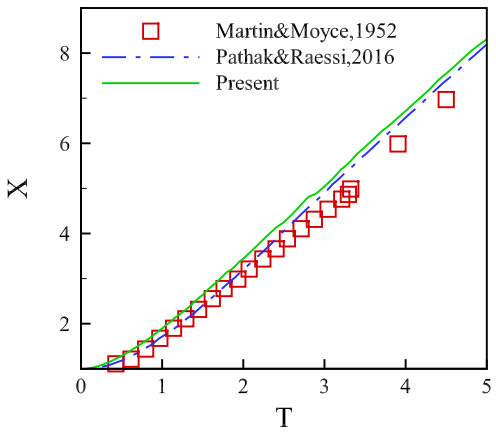


Fig. 6: The dimensionless wave front varies with dimensionless time in the collapsing water column.

Copyright © 2021 by JSFM

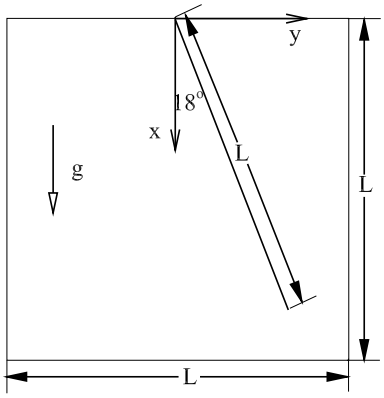


Fig. 7: Computational configuration of pendulum hanging in vacuum.

rigidity, K_b, equalling 0.01 and Froude number, Fr, equalling 0.1. The initial conditions are set as,

$$\mathbf{X}(s,0) = \mathbf{X}_0 + (L-s)(\cos k, \sin k). \tag{14}$$

$$\partial \mathbf{X}(s,0)/\partial t = (0,0). \tag{15}$$

The boundary conditions are fixed end and free end, respectively, written as,

$$\mathbf{X}(s,t) = (0,0),\ \frac{\partial^2 \mathbf{X}(s,t)}{\partial s^2} = (0,0). \tag{16}$$

$$T = 0,\ \frac{\partial^2 \mathbf{X}(s,t)}{\partial s^2} = (0,0),\ \frac{\partial^3 \mathbf{X}(s,t)}{\partial s^3} = (0,0). \tag{17}$$

Figure. 8 shows the evolution of the position in the direction perpendicular to gravity of hanging pendulum with time changing. The results show great agreement with previous numerical solution[23].

5. Application

5.1 Flow past filament

We investigate here the dynamics of uniform flow past a fleible filament, to examine the performance of the method in simulating the coupling of fluid flow with structure motion and deformation. We consider the configuration with the filament pinned at the leading edge and let the trailing edge free of internal structural forces.

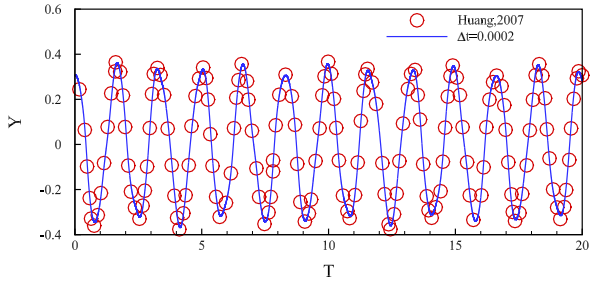


Fig. 8: The dimensionless free end position of hanging pendulum varies with dimensionless time.

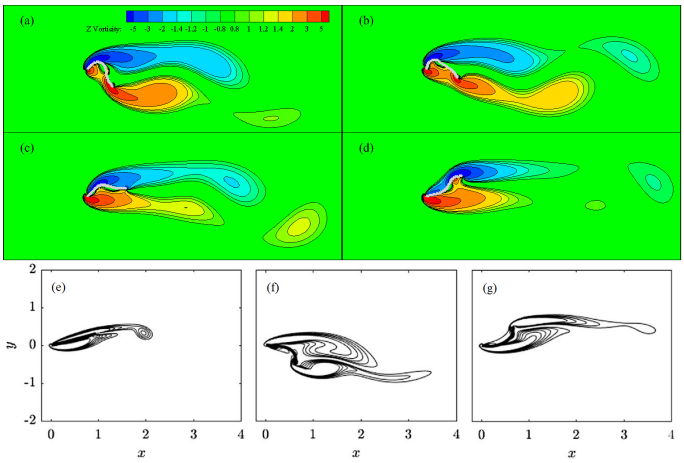


Fig. 9: Vorticity contours of a uniform flow over a filament with $Re = 50$, $K_b = 0.0001$, and $\rho_s/\rho L = 50$ at dimensionless time $T =$ (a) 42, (b) 44.4, (c) 46.8, and (d) 49.2, and with $Re = 200$, $K_b = 0.0015$, and $\rho_s/\rho L = 100$ at dimensionless time $T =$ (e) 1.2, (f) 18, and (g) 31.2 in Goza's work[41].

We choose L and U as the characteristic length and velocity. The computational domain is 8×8. The left boundary is inflow boundary condition with constant velocity U. The right boundary is convective boundary condition. Both upper and lower boundaries are no-penetration boundary condition. We simulate the flows with mesh size $\Delta x = 0.01L$ and time step $\Delta t = 0.0002$ at $Re = 50$, $K_b = 0.0001$, and $\rho_s\ \rho L = 50$.

Figure 9 shows the vorticity contours of the flow past filament with qualitative comparison with previous numerical results[41]. It is obvious that the flapping process is significant with large amplitude with regard to the fixed-point stability regime and limit-cycle flapping regime in previous work[22]. This is due to the massive effect, with structure-to-fluid density ratio, 50, in present case and, 100, in Goza's simulation[41]. In addition to fierce and chaotic flapping, thick, wild, and irregular wake profiles are also observed. The destabilizing effect of increasing mass ratio was discussed in

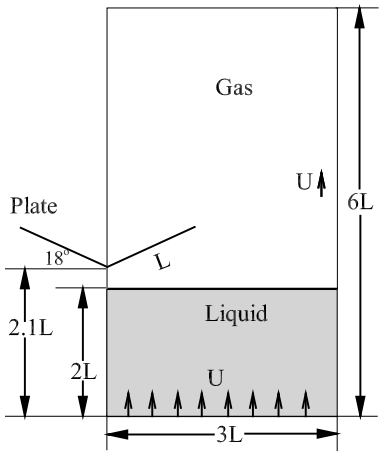


Fig. 10: Computational configuration of hydroelastic water entry of a flexible plate.

Copyright © 2021 by JSFM

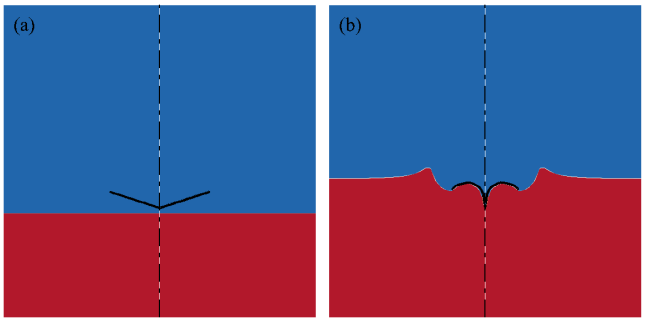


Fig. 11: Deformation of free surface and flexible plate with $Re = 50$, $K_b = 0.0001$, and $\rho_s/\rho L = 150$ at dimensionless time $T =$ (a) 0.0 and (b) 0.64.

previous work[22]. Regardless of the asymmetric vortex pattern, positive and negative vortex are still formed in a staggered way in both case.

5.2 Hydroelstic water entry

We consider here a flexible plate plunging into a water pool at constant velocity, to verify the performance of the model in the simulation of interaction between multiphase interface and flexible solid structure. In this flow phenomenon, the impact dynamics is characterized by the deformation of the free surface, including the formation of crater[42] under water and the ejacta[43] or splash[44] as crown structure in periphery. Despite extensive research in the topic, most previous studies were focusing on the impact of rigid solid body with a unchanging geometry boundary, and there is still a lack of investigation on water entry dynamics with deformable structure.

In our studies the relative dimensionless number are Reynolds number, Re, bending rigidity, K_b, and structure-to-fluid density ratio $\rho_s/\rho L$, where the flexible plate length L, the impact speed U, and the physical properties of liquid are chosen as corresponding characteristic quantities. Here, we assure the flexible plate impact the water pool with a constant velocity at early stage from contact water pool, which was also observed in previous experiments[45] and the gravity, together with capillary, are also ignored. For the convenience of

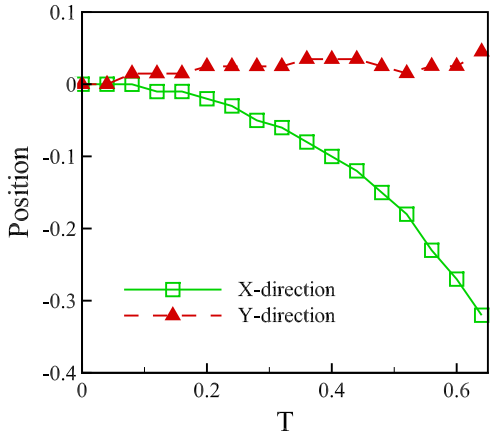


Fig. 12: The evolution of displacement at free end with time in both horizontal (X) and vertical (Y) direction.

computation, instead of letting the plate falling freely, we fix the plate and let the liquids go upwards at a speed of U as shown in Figure. 10. All the computations are performed in a domain of 3×6 with a mesh size of $\Delta x = 0.01L$. The flexible plate is placed at a height of $2.1L$ from the bottom of the domain.

Figure. 11 shows the numerical results of the shape of free surface and the deformation of flexible plate at time of $T = 0.0$ and 0.64 with $Re = 50$, $K_b = 0.0001$ and $\rho_s/\rho L = 150$. The density of liquid to that of gas is set to be 1000. As can be seen in Figure. 10, at initial moment, the plate is in a wedge shape with deadrise angle equaling 18^o. At $T = 0.64$, the flexible plate bends into a shape of "Asagao" under pressure and viscous stress from the liquid below. The plate is fixed one end, and the other end is free of tensile, bending and shear force and under the constraints of inextensibility. In Figure. 12 the relative displacements to initial position of free end are depicted in both horizontal and vertical directions. It is obviously that, in early stage of impact, the free end only elevates slightly in vertical direction but contracts drastically in horizontal direction due to large tensile force inside the plate tracking free end towards symmetrical axis.

6. Conclusion

A constrained interpolation profile immersed boundary method has been proposed for the simulation of interaction between free-surface flow and flexible structure. In this method, using constrained interpolation profile method, we can track the immiscible interface of two fluid with large density ratio up to 1000. A geometrical nonlinear structure is also solved implicitly with small bending rigidity and large tensile force, which keep the structure inextensible. Furthermore, With the help of immersed boundary method, we can use non-comformal mesh such as Cartesian mesh to simulate interaction between free-surface flows with deformable flexbile structure with complex geometries. Our numerical tests showed that the approach can produce converged results with mesh refinement regarding to hydrodynamic force calculation. The performance of the approach has been examined through a variety of numerical experiments: flow past circle cylinder was simulated and agreed well with the numerical results in literature. The dynamic evolution of free surface in a dam break flow appear to be in agreement with previous laboratory experiments and numerical results. A variety of dynamic of deformation of flexible Euler-Bernoulli structure with or without coupling of flow field was investigated, including a hanging pendulum in vacuum, and the results were consistent with others numerical results. The applications of flow past filament and hydroelastic water entry of flexible plate were also revealed.

References

(1) Hepf, H. M., "Flow and transport in regions with aquatic vegetation," Annu. Rev. Fluid Mech., 44 (2012), pp. 123-142.

(2) Feltham, D. L., "Sea ice rheology," Annu. Rev. Fluid Mech., 40 (2008), pp. 91-112.

(3) Py, C., "Capillary origami: Spontaneous wrapping of a droplet with an elastic sheet," Phys. Rev. Lett., 98 (2007), 156103.

(4) Harlow, F. H., Welch, J. E., "Numerical calculation of time dependent viscous incompressible flow of

Copyright © 2021 by JSFM

fluid with free surface," Phys. Fluids, 8 (1965), 2182.

(5) Unverdi, S. O., Tryggvason, Gretar, "A front-tracking method for viscous, incompressible, multi-fluid flows," J. Comput. Phys., 100 (1992), pp. 25-37.

(6) Tryggvason G., Bunner, B., Esmaeeli, A., Juric, D., Al-Rawahi, N., Tauber, W., Han, J., Nas, S., Jan, Y. J., "A front tracking method for the computations of multiphase flow," J. Comput. Phys., 169 (2001), pp. 708-759.

(7) Sussman, M., Almgren, J. B., Bell, J. B., Colella, P., Howell, L. H., Welcome, M. L., " An adaptive level set approach for incompressible two-phase flows," J. Comput. Phys., 148 (1999), pp. 81-124.

(8) Osher, S., Fedkiw, R. P., " Level set methods: an overview and some recent results," J. Comput. Phys., 169 (2001), pp. 463-502.

(9) Hirt, C., Nichols, B., "Volume of fluid (VOF) method for the dynamics of free boundaries," J. Comput. Phys., 39 (1981), pp. 201-225.

(10) Scardovelli, R., Zaleski, S., "Direct numerical simulation of free-surface and interfacial flow," Annu. Rev. Fluid Mech., 31 (1999), pp. 567-603.

(11) Anderson, D. M., McFadden, G. B., Wheeler, A. A., "Diffuse-interface methods in fluid mechanics," Annu. Rev. Fluid Mech., 30 (1998), pp. 139-165.

(12) Jacqmin, D., "Calculation of two-phase Navier–Stokes flows using phase-field modeling," J. Comput. Phys., 155 (1999), pp. 96-127.

(13) Yabe, T., Aoki, T., "A universal solver for hyperbolic equations by cubic-polynomial interpolation I. One-dimensional solver," Comput. Phys. Commun., 66 (1991), pp. 219-232.

(14) Yabe, T., Ishikawa, T., Wang, P. Y., Aoki, T., Kadota, Y., Ikeda, F., "A universal solver for hyperbolic equations by cubic-polynomial interpolation II. Two- and three-dimensional solvers," Comput. Phys. Commun., 66 (1991), pp. 233-242.

(15) Fukumitsu, K., Yabe, T., Ogata, Y., Oami, T., Ohkubo, T., "A new directional-splitting CIP interpolation with high accuracy and low memory consumption," J. Comput. Phys., 286 (2015), pp. 62-69.

(16) Peskin C. S., "Flow patterns around heart valves: A numerical method," J. Comput. Phys., 10 (1972), pp. 252-271.

(17) Peskin C. S., "Numerical analysis of blood flow in the heart," J. Comput. Phys., 25 (1977), pp. 220-252.

(18) Kim, Y., Peskin, C. S., "Penalty immersed boundary method for an elastic boundary with mass," Phys. Fluids, 19 (2007), 053103.

(19) Kim, Y., Lai, M. C., "Simulating the dynamics of inextensible vesicles by the penalty immersed boundary method," J. Comput. Phys., 229 (2010), pp. 4840-4853.

(20) Mohd-Yusof, J., "Combined immersed boundary/B-spline methods for simulations of ow in complex geometries," CTR Annu. Res. Briefs, (1997), pp. 317-327.

(21) Ren, W. W., Shu, C., Wu, J., Yang, W. M., "Boundary condition-enforced immersed boundary method for thermal flow problems with Dirichlet temperature condition and its applications," Comput. Fluids, 57 (2012), pp. 40-51.

(22) Connell, B. S., Yue, D. K., "Flapping dynamics of a flag in a uniform stream," J. Fluid Mech., 25 (1977), pp. 220-252.

(23) Huang, W. X., Shin, S. J., Sung, H. J., "Simulation of flexible filaments in a uniform flow by the immersed boundary method," J. Comput. Phys., 226 (2007), pp. 2206-2228.

(24) Bico, J., Reyssat, E., Roman, B., "Elastocapillarity: When surface tension deforms elastic solids," Annu. Rev. Fluid Mech., 50 (2018), pp. 629-659.

(25) Gingold, R. A., Monaghan, J. J., "Smoothed particle hydrodynamics - theory and application to non-spherical stars," Mon. Not. R. Astron. Soc., 181 (1977), pp. 375-389.

(26) Monaghan, J. J., "Smoothed particle hydrodynamics and its diverse applications," Annu. Rev. Fluid Mech., 44 (2012), pp. 323-346.

(27) Zhang, G., Hu, T., Sun, Z., Wang, S., Shi, S., Zhang, Z., "A δSPH–SPIM coupled method for fluid–structure interaction problems," J. Fluid Struct., 101 (2021), 103210.

(28) Koshizuka, S., Oka, Y., "Moving particle semi-implicit method for fragmentation of incompressible fluid," Nucl. Sci. Eng., 123 (1996), pp. 421-434.

(29) Khayyer, A., Gotoh, H., Shimizu, Y., Nishijima, Y., "A 3D Lagrangian meshfree projection-based solver for hydroelastic fluid–structure interactions," J. Fluid Struct., 105 (2021), 103342.

(30) Liao, K., Hu, C., "A coupled FDM–FEM method for free surface flow interaction with thin elastic plate," J. Mar. Sci. Technol., 18 (2013), pp. 1-11.

(31) Xiao, F., Honma, Y., Kono, T., "A simple algebraic interface capturing scheme suing hyperbolic tangent function," Int. J. Numer. Methods Fluids, 48 (2005), pp. 1023-1040.

(32) Yang, L., Gil, A. J., Carreno, A. A., Bonet, J., "Unified one-fluid formulation for incompressible flexible solids and multiphase flows: Application to hydrodynamics using the immersed structural potential method (ISPM)," Int. J. Numer. Mech. Fluids, 86 (2018), pp. 78-106.

(33) He, S., Yang, Z., Sotiropoulos, F., Shen, L., "Numerical simulation of interaction between multiphase flows and thin flexible structures," J. Comput. Phys., 448 (2022), 110691.

(34) Liu, H. R., Ding, H., "A diffuse-interface immersed-boundary method for two-dimensional simulation of flows with moving contact lines on curved substrates," J. Comput. Phys., 294 (2015), pp. 484-502.

Copyright © 2021 by JSFM

(35) Lima, A. L. F., Silva, E., Silveira-Neto, A., Damasceno, J. J. R., "Numerical simulation of two-dimensional flows over a circular cylinder using the immersed boundary method," J. Comput. Phys., 189 (2003), pp. 351-370.

(36) Xu, S., Wang, Z. J., "An immersed interface method for simulating the interaction of a fluid with moving boundaries," J. Comput. Phys., 216 (2006), pp. 454-493.

(37) Wang, Z., Fan, J., Cen, K., "Immersed boundary method for the simulation of 2d viscous flow based on vorticity-velocity formulation," J. Comput. Phys., 228 (2009), pp. 1504-1520.

(38) Liu, H. R., Gao, P., Ding, H., "Fluid–structure interaction involving dynamic wetting: 2D modeling and simulations," J. Comput. Phys., 348 (2017), pp. 45-65.

(39) Pathak, A., Raessi, M., "A 3D, fully Eulerian, VOF-based solver to study the interaction between two fluids and moving rigid bodies using the fictitious domain method," J. Comput. Phys., 311 (2016), pp. 87-113.

(40) Martin. J., Moyce. W., "An experimental study of the collapse of liquid columns on a rigid horizontal plane," Philos. Trans. R. Soc. Lond., 244 (1952), pp. 312–324.

(41) Goza, A., Gao, Colonius, T., "A strongly-coupled immersed-boundary formulation for thin elastic structures," J. Comput. Phys., 336 (2017), pp. 401-411.

(42) Wang, A., Duncan, J. H., "The controlled vertical impact of an inclined flat plate on a quiescent water surface," J. Fluid Mech., 879 (2019), pp. 468-511.

(43) Mayer, H. C., Krechetnikov, R., "Flat plate impact on water," J. Fluid Mech., 850 (2018), pp. 1066-1116.

(44) Peters, I. R., van der Meer, D., Gordillo, J. M., "Splash wave and crown breakup after disc impact on a liquid surface," J. Fluid Mech., 724 (2013), pp. 553-580.

(45) Ding, H., Chen, B. Q., Liu, H. R., Zhang, C. Y., Gao, P., Lu, X. Y., "On the contact-line pinning in cavity formation during solid–liquid impact," J. Fluid Mech., 783 (2015), pp. 504-525.

Copyright © 2021 by JSFM